IL NUOVO CIMENTO Vol. 30 C, N. 5 Settembre-Ottobre 2007
DOI 10.1393/ncc/i2008-10260-2

Development of Silicon PhotoMultipliers at FBK-irst(*)

C. Piemonte[1](**), R. Battiston[2], M. Boscardin[1], G.-F. Dalla Betta[3], A. Del Guerra[4], G. Llosa[4], M. Melchiorri[2], A. Pozza[1] and N. Zorzi[1]

([1]) *Fondazione Bruno Kessler (FBK)-irst - Via Sommarive, 18, I-38050 Povo (Trento), Italy*
([2]) *INFN, Sezione di Perugia and Università di Perugia - Via A. Pascoli I-06123 Perugia, Italy*
([3]) *INFN, Sezione di Padova (Gruppo Collegato di Trento) and Università di Trento Via Sommarive 14, I-38050 Povo (Trento), Italy*
([4]) *INFN, Sezione di Pisa and Università di Pisa - Largo Pontecorvo 3, I-56127 Pisa, Italy*

(ricevuto il 3 Marzo 2008; pubblicato online il 23 Aprile 2008)

Summary. — We report on the development of Silicon PhotoMultipliers (SiPM) at the Fondazione Bruno Kessler (FBK)-irst (Trento, Italy) in the framework of a collaboration with INFN. Device geometry and technology are resumed, and selected results from the characterization of SiPM prototypes from three production batches are reported, including static, dynamic, and noise properties, as well as photodetection efficiency.

PACS 29.40.Wk – Solid-state detectors.
PACS 85.30.De – Semiconductor-device characterization, design, and modeling.
PACS 85.30.Mn – Junction breakdown and tunneling devices (including resonance tunneling devices).
PACS 85.60.Gz – Photodetectors (including infrared and CCD detectors).

1. – Introduction

The Silicon PhotoMultiplier (SiPM) is a new type of solid-state photodetector consisting in a matrix of tiny passive-quenched Geiger-mode avalanche photodiodes (that will be referred to as micro-pixels) all connected in parallel, providing a large current signal and a wide dynamic range, up to few hundred photons (see [1] and references therein). SiPMs have recently been the object of increasing interest from the scientific community as they represent a very advantageous alternative to vacuum-based photomultiplier tubes

(*) Paper presented at the 1st Workshop on Photon Detection for High Energy Medical and Space Applications; Perugia, June 13-14, 2007.
(**) E-mail: piemonte@itc.it

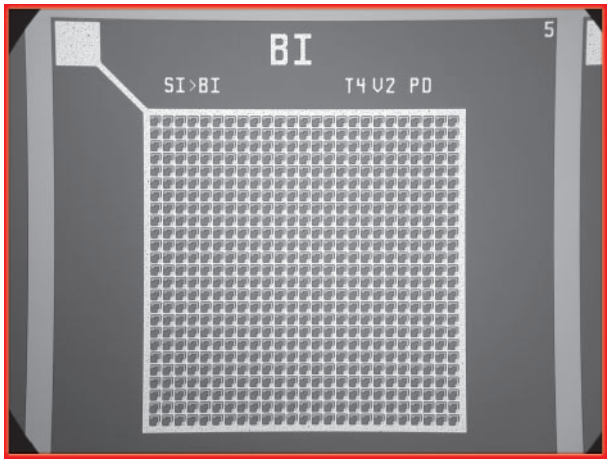

Fig. 1. – Photograph of a 1 mm^2 SiPM prototype produced at FBK-irst.

in many applications, due to their compactness, ruggedness, low operational voltage, insensitivity to magnetic fields and low cost. Nevertheless, two main drawbacks, namely their sensitivity to temperature variations and their relatively low radiation resistance, should be taken into account when thinking of their applications.

Since 2005, FBK-irst has been involved in an R&D activity on Silicon Photomultipliers (SiPMs) in the framework of a collaboration with INFN focused on the technological development and application of SiPMs in calorimetry, Time-Of-Flight and Positron Emission Tomography (PET). So far, three mini batches of SiPM prototypes have been produced in the fabrication laboratory of FBK-irst with the aim of tuning the technology and improving the performance. An extensive characterization work has been carried out on these devices in order to verify the functioning, the noise and optical characteristics, as well as the process uniformity and reproducibility. This paper reports on the device geometrical and technological features as well as on selected results from the electro-optical characterization.

2. – Device description

Our first SiPM prototypes have 25×25 micro-pixels, each with a $40\times40\,\mu$m^2 area, so as to cover a total area of 1 mm^2. A photograph of the device is shown in fig. 1. The micro-pixels are all connected in parallel by a metal grid on the front-side and by the substrate of the epitaxial silicon on the back-side. The basic micro-pixel structure is an n^+-p junction, where an additional p-type layer is used to fix the breakdown voltage, and a high-ohmic polysilicon resistor in series. A schematic cross-section of the micro-cell is shown in fig. 2. These SiPMs have been specially designed to be efficient at short wavelength, so as to match the light emission properties of LSO scintillator that is typically used in PET [2]. To this purpose, the device features: i) a thin epitaxial layer ($4\,\mu$m); ii) a very shallow junction ($\simeq 100$ nm); iii) an optimized anti-reflective coating (ARC) yielding an almost 100% light transmission efficiency at wavelengths around 420 nm.

In the standard prototypes, no additional structure to prevent optical cross-talk between micro-cells is present. Only recently we started to address this issue in some wafers

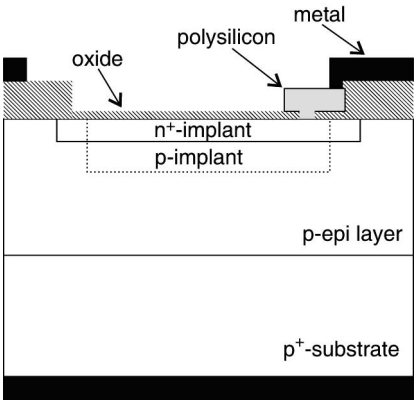

Fig. 2. – Schematic cross-section of a micro-pixel (not to scale).

by implementing an optical isolation structure consisting in trenches covered with aluminum to avoid the transmission of photons to adjacent micro-cells. More details on the device can be found in [3, 4].

Three batches have been produced using the same wafer layout in order to focus only on the technological development. In this phase, no attempt has been devoted to optimize the device geometry, and as a consequence the area efficiency (fill factor), leaving this issue to the next productions. This must be kept in mind since the fill factor is one of the main factors limiting the photodetection efficiency of the device. In particular, the fill factor is mainly determined by the dead area present at the borders of each micro-cell composing the SiPM with an additional loss possibly arising from the polysilicon resistor and the metal lines.

Neglecting for simplicity the second contribution, the maximum fill factor achievable for a dead border region of 4 and 6 μm, respectively, is shown in fig. 3. At a size of the micro-pixel of 40 μm (*i.e.* the same as in our prototype), the maximum fill factor is

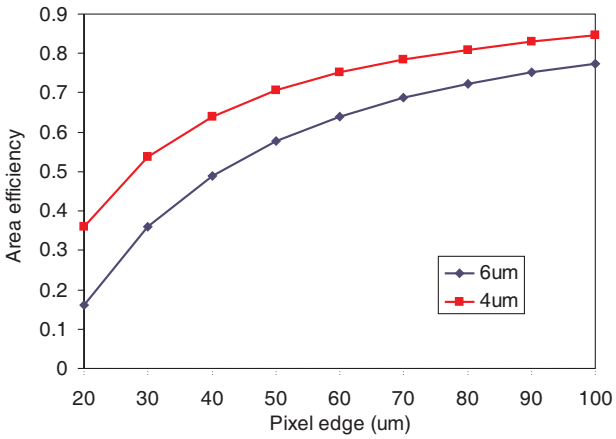

Fig. 3. – Fill factor as a function of the micro-pixel edge size for two different technologies having a border region of 4 and 6 μm, respectively.

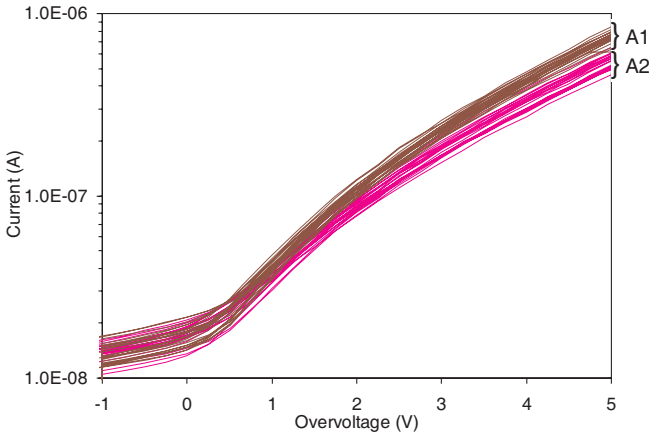

Fig. 4. – SiPM current as a function of the overvoltage. Two groups of devices can be distinguished, which differ in the size of the high-field region.

almost 50% even with a 6 μm edge size, whereas at present we have two layout versions with fill factor of 20 and 30%, respectively (a large fraction of the dead area is indeed due to the polysilicon resistor). Thus, there is room for an improvement and with a new design we actually reached a fill factor higher than 40%. Of course with larger pixels it is easier to increase the fill factor, but this comes at the expense of a lower dynamic range for a given total area.

3. – Device characterization

3˙1. *I-V measurement*. – In spite of its simplicity, the static current-voltage (I-V) measurement in dark condition can provide useful information on the functioning of the device, and is indeed a fast and reliable sorting tool in case of large productions. In particular, the relevant parameters that can be extracted from reverse I-V curves are the breakdown voltage and the dark noise level. As reported in [3], the current above the breakdown is given by the charge of the dark pulses times the number of dark pulses per second. Assuming the number of events affected by optical cross-talk and after-pulses to be negligible, the charge associated to each dark pulse is proportional to the gain of the device. Thus, the static current at a given voltage above breakdown is given by the product of the gain of the device and the dark count rate.

More than 1000 devices coming from the three batches have been measured. As an example, fig. 4 shows the current as a function of the overvoltage (*i.e.* the difference between the bias voltage and the breakdown voltage) for two sets of devices having a different size of the high-field region. Measurements were performed at room temperature. In total, 57 out of 63 devices coming from one wafer are shown. As can be seen from fig. 4, at a given gain value, the I-V curves are very uniform so that the dark count rate is expected to be very uniform as well. The current of the 6 devices from the same wafer not shown in the plot presents an anomalous behavior, *i.e.* either a premature breakdown voltage or a higher (more than twice) post-breakdown current level. Concerning the breakdown voltage, which is around 30 V, we found a maximum variation within a wafer of about 1 V. Slightly higher variations (2–3 V) can be observed on devices coming from different batches.

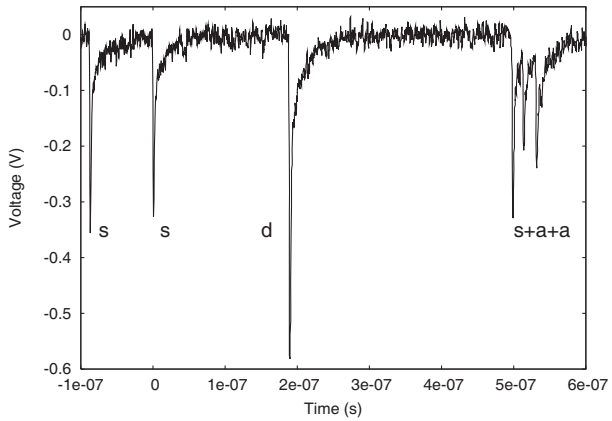

Fig. 5. – Different types of signals observed on the scope: s = single pulse, d = double pulse, a = after-pulse.

3˙2. *Signal and noise characterization.* – The dynamic characterization of the device in dark condition is extensively treated in [3]. Here, for the sake of clarity, we report some of the main results. About 100 samples have been bonded to a standard transistor package and tested using a very simple read-out electronics: the SiPM is connected to ground through a 50Ω resistor and the voltage drop on the resistor is amplified with a wide-band voltage amplifier. The output signals of the amplifier are then monitored on a digital scope. Three types of signals can be observed (see fig. 5): i) single pulses coming from the activation of one micro-cell; ii) double pulses corresponding to events affected by optical cross-talk, and iii) pulses immediately followed by smaller pulses due to the release of carriers trapped during the first avalanche (after-pulsing phenomenon). Integrating the signals over a time of 100 ns in order to include the whole recovery of the micro-cell, the spectrum shown in fig. 6 can be obtained. The main peak corresponding to single pulses can be very well fitted by a Gaussian function (solid line), whose standard deviation is

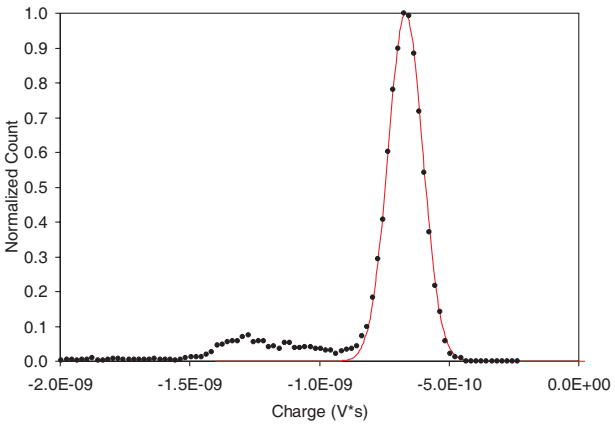

Fig. 6. – Charge spectrum of a SiPM. The integration time is 100 ns and the overvoltage is 3 V.

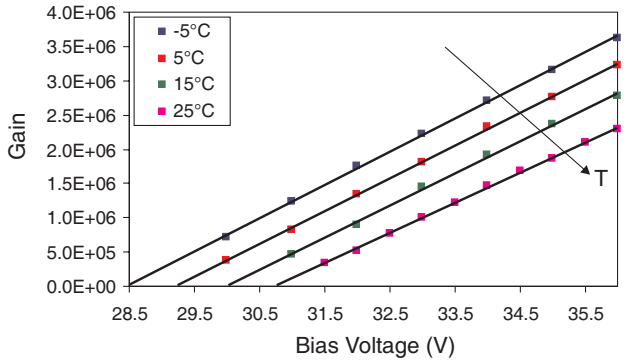

Fig. 7. – Gain as a function of the bias voltage at different temperatures.

given by the noise introduced by the read-out chain and by small gain non-uniformities of the micro-cells composing the SiPM. The tail is determined by events presenting excess charge, namely, pulses affected by optical cross-talk and/or after-pulses: the former give events with twice the charge of single pulses, the latter give values randomly distributed above the single-pulse value. As for the optical cross-talk, although no optical isolation is present between micro-cells, its probability never exceeds 10% even at large overvoltage values, owing to the thin epitaxial layer. Nevertheless, preliminary measurements on the prototypes featuring trenches between the micro-cells have indeed shown a much lower optical cross-talk probability (almost one order of magnitude lower).

Other tests have been performed in a climatic chamber with temperature ranging from $-5\,^{\circ}\mathrm{C}$ to $25\,^{\circ}\mathrm{C}$. The temperature dependence of the breakdown voltage is indeed an important issue, leading to large gain variation at a fixed bias voltage. The gain of the device as a function of the bias voltage at different temperatures in shown in fig. 7: the breakdown voltage can be determined from the intercept of the linear fit of the gain-voltage characteristic with the x-axis. In all cases, the gain increases linearly with the bias voltage and reaches a value of 10^6 at about 3 V overvoltage. The temperature dependence of the breakdown voltage and of the gain can be better appreciated in fig. 8. From the linear fit, a breakdown voltage variation of about 80 mV/K (corresponding to 2.7%/K) can be obtained, in good agreement with theoretical predictions [5].

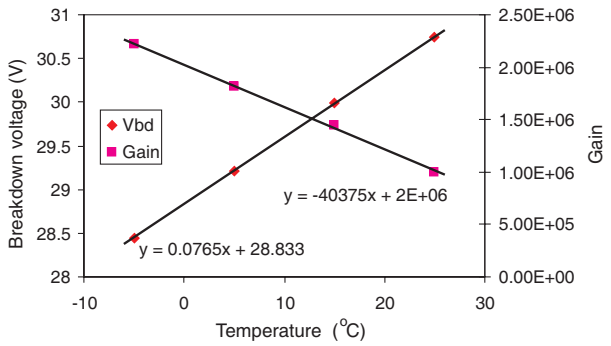

Fig. 8. – Breakdown voltage and gain at 3 V overvoltage *vs.* temperature.

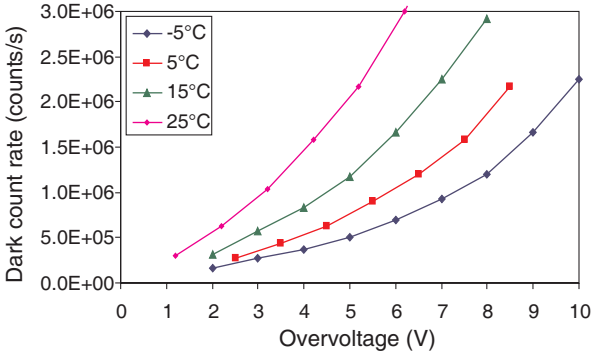

Fig. 9. – Dark count rate as a function of the overvoltage at different temperatures.

The temperature variation also affects the dark count rate because of the change in the carrier thermal generation rate, as predicted by Shockley-Read-Hall theory [5]. This is confirmed by fig. 9, showing the dark count rate as a function of the overvoltage at different temperatures. At room temperature, the dark count rate is in the order of 1 MHz at 3 V overvoltage, and it decreases at lower temperature due to a lower thermal generation. These values are good enough for many applications, but they could be further reduced by means of optimized gettering techniques, that we have started to develop. Preliminary results from samples treated with polysilicon-based gettering are encouraging, with a dark count rate reduction of about 70%.

3˙3. *Photodetection efficiency measurement.* – The photodetection efficiency (PDE) measurement completes the characterization of our device. We used the optical bench at FBK-irst equipped with: a white-light source, attenuation filters and a monochromator. First, we calibrated every filter and the light from the monochromator for a set of wavelengths ranging from 380 nm to 700 nm (using a calibrated diode). Then, we attenuated the light with the calibrated filters in order to have some 10^7 photons/s/mm^2, a light intensity which allows to avoid saturation effects in the SiPM. The measurement has been performed by using two different methods. In the first method we measured the DC current under illumination. The difference between this value and the DC current in dark condition is proportional to the number of detected photons, the proportionality factor being the gain of the SiPM which was previously determined. This is a very simple static measurement but it requires the evaluation of the gain. In order to confirm the validity of this method we performed a second test using the device as a photon counter, *i.e.* we counted the number of pulses per second. After subtracting the number of dark counts, this is the number of detected photons. Such a method gives a direct measurement of the PDE but requires the presence of a more complicated read-out chain. Notably, we found a very good agreement between these two techniques. The resulting photodetection efficiency as a function of the wavelength for a device having a fill factor of 0.2 is shown in fig. 10. The measurement has been performed at different overvoltage values, ranging from 2 to 4 V.

In order to understand the shape of the plots in fig. 10 we have to remind that the PDE is given by the product of three factors: the fill factor (A_e), the quantum efficiency (QE) and the avalanche triggering probability (P_t). The first term is independent of the bias voltage as well as from the light wavelength (λ). Thus, it corresponds to an upper

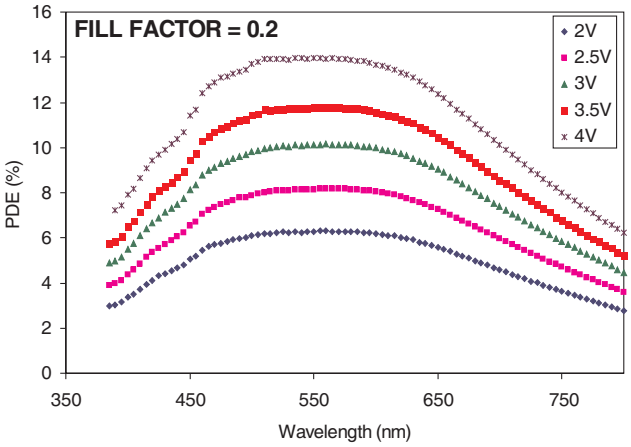

Fig. 10. – PDE *vs.* wavelength at different overvoltages from 2 V to 4 V.

limit for the PDE that in the measured device is 0.2. The contribution of P_t has been explained in detail in [4]: it is worth recalling that it depends both on the bias voltage, because the impact ionization rates increase with the electric field, and on λ, because the triggering probability is not constant throughout the depletion depth. The latter effect can be better understood with the aid of fig. 11: if the avalanche is triggered by holes, which is the case at short wavelengths in our device, the triggering probability is about one half with respect to that of electrons (long wavelengths). Finally, the QE depends on λ because both the transmission efficiency of the anti-reflective coating and the internal quantum efficiency (that is the probability for a photogenerated carrier to reach the high-field region) depend on the wavelength.

In summary, the PDE dependence on the bias voltage has to be attributed to the triggering probability, whereas the PDE dependence on the light wavelength is a mixed contribution from P_t and QE. To understand in detail this point, we measured the quantum efficiency directly on some diodes extracted from the same wafers, and having

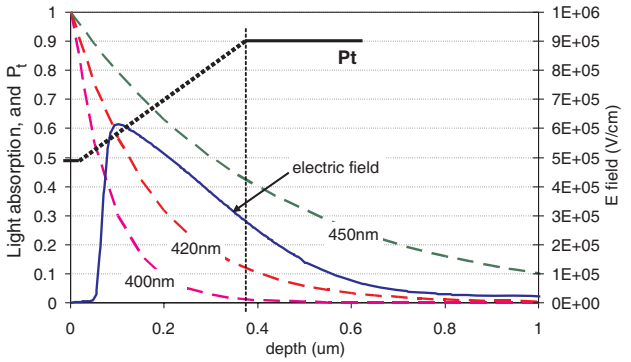

Fig. 11. – Normalized light absorption and electric field as a function of depth. The trend of P_t *vs.* depth is also shown.

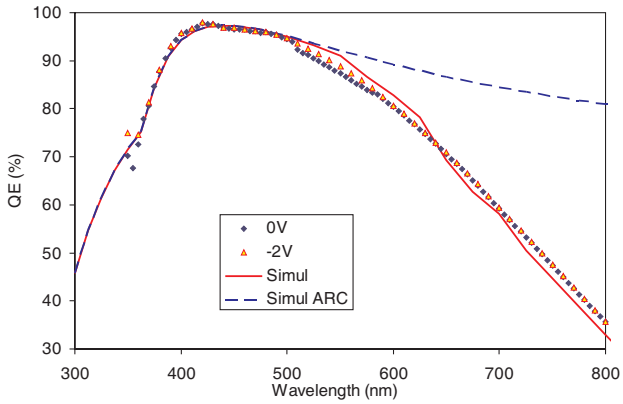

Fig. 12. – QE *vs.* wavelength in a 1 mm^2 diode having the same doping profiles and anti-reflective coating of the SiPM.

the same anti-reflective coating and doping profiles as the SiPM. The outcome of this test is shown in fig. 12. The measurement has been performed at different bias voltages: from 0 to 5 V. Up to 3 V we obtain the same curve, whereas for higher biases the QE starts increasing because of impact ionization (note that the breakdown voltage is 30 V). Notably, due to our technological choices, the QE is higher than 90% for wavelengths ranging from 380 to 530 nm. TCAD simulations of the QE had been previously carried out to tune the technology and the agreement is indeed very good (see solid line in fig. 12). The simulated transmittance of the ARC is shown in fig. 12 as well (dashed line). It can be noticed that the decrease of QE at short λ is caused by the poor transmittance of the ARC, while at long λ the small thickness of the epitaxial layer determines the QE decrease. Hence, the PDE at long light wavelengths decreases because the QE is reduced. On the other hand, at wavelengths around 400 nm the PDE has already reached a minimum while the QE is still at its maximum. This means that for wavelengths ranging from 350 to 450 nm the triggering probability is the main factor limiting the PDE. It is worth stressing that, among the factors determining the photodetection efficiency, the triggering probability is the only one that cannot be directly measured. Yet it can be determined analytically from the other measured parameters. By doing so, the P_t has been found to reach its maximum for $\lambda > 550$ nm, while the minimum constant level is reached for $\lambda < 400$ nm. The ratio between the maximum and minimum values is about 2, as predicted by theory. The absolute values of P_t of course depend on the bias voltage, and so does PDE.

4. – Conclusions

We have reported on the development of Silicon PhotoMultipliers at FBK-irst. Results from the first productions are indeed very encouraging. The technology has demonstrated to be reliable since the device is working properly and its performance is reproducible from batch to batch. Further work is ongoing on the technological side to reduce the dark noise and to increase the photodetection efficiency at short wavelengths. Recent developments involve also the geometrical optimization, and a new batch of devices was recently completed which includes SiPM and small SiPM matrices with a larger area and

an optimized fill factor. The characterization of this batch is under way and will be the object of a forthcoming paper.

* * *

This work has been partially supported by the Provincia Autonoma di Trento (PAT) and by the National Institute of Nuclear Physics of Italy (INFN) under the Framework Program "MEMS" and the V Scientific Commission Projects DASIPM and DASIPM2.

REFERENCES

[1] Buzhan P., Dolgoshein B., Ilyin A., Kantserov V., Kaplin V., Karakash A. *et al.*, *ICFA Intrumentation Bull.*, **23** (2001) 28.
[2] Llosa G., Battiston R., Bisogni M. G., Boscardin M., Collazuol G., Corsi F. *et al.*, *Novel Silicon Photomultipliers for PET application*, in *IEEE Nuclear Science Symposium and Medical Imaging Conference, Conference Record, San Diego, CA (USA), Oct. 29-Nov. 4, 2006*, paper M06-88.
[3] Piemonte C., Battiston R., Boscardin M., Dalla Betta G.-F., Del Guerra A., Dinu N., Pozza A. and Zorzi N., *IEEE Trans. Nucl. Sci.*, **54** (2007) 236.
[4] Piemonte C., *Nucl. Instrum. Methods Phys. Res. A*, **568** (2006) 224.
[5] Sze S. M., *Physics of Semiconductor Devices* (John Wiley & Sons, N.Y.) 1981.